Laminated Iron-Core Inductor Model for Time-Domain Analysis

G. Grandi[1], A. Massarini[2], U. Reggiani[1], and G. Sancineto[1]

(1) Dept. of Electrical Engineering, University of Bologna
Viale Risorgimento 2, 40136 - Bologna, Italy

(2) Dept. of Engineering Sciences, University of Modena and Reggio Emilia
Via Vignolese 905, 41100 - Modena, Italy

***Abstract*— The development of new power electronic components and soft switching techniques has allowed an increase in the switching frequency reducing the size of inductors and capacitors. Magnetic components are employed in most switching converters so a renewed attention is paid to inductors and transformers with particular emphasis to the high-frequency behavior of the winding and core, and the effects of parasitic capacitances. Laminated iron-core inductors are largely used in the medium to high power range as choke coils, filtering devices and link coils. In this paper, a model for laminated iron-core inductors is developed for studying electromagnetic transients. The proposed model allows time-domain analysis to be performed by means of standard circuit-oriented simulation programs.**

***Index Terms*—Inductors, eddy currents, iron, electromagnetic transient analysis, circuit analysis.**

I. Introduction

The development of new power electronic components and soft switching techniques has allowed an increase in the switching frequency reducing the size of employed inductors and capacitors. Nowadays, the nonideal high-frequency behavior of passive components needs to be investigated to characterize the parasitic elements which cause the shifting of the behavior from the ideal one. Models are useful to predict the high-frequency behavior of power electronic devices in the frequency range from tens of kHz to MHz. Magnetic components are employed in most switching converters so a renewed attention is paid to inductors and transformers with particular emphasis to the behavior of the winding and core, and the effects of parasitic capacitances.

Laminated iron-core inductors are largely used in the medium to high power range as choke coils, filtering devices and link coils. High-frequency models of inductors have been developed in [1], [2], [3] where skin and proximity effects in the winding, eddy currents in the core, turn-to-turn and turn-to-iron capacitances have been taken into account. The structure of the equivalent circuits proposed in the above-mentioned papers is shown in Fig. 1. Since the ac resistance and inductance of the model are frequency-dependent, the equivalent circuits depicted in Fig. 1 can be used for frequency-domain analysis, whereas time-domain analysis is possible only through inverse Laplace or Fourier transform

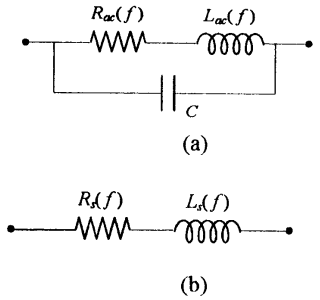

Fig. 1. (a) Lumped equivalent circuit of the inductor with frequency-dependent parameters. (b) Series equivalent circuit.

techniques. In this paper, a model suitable for a direct analysis of electromagnetic transients is developed for laminated iron-core inductors. The winding model is based on a series Foster circuit [4] that is fitted by the Dowell's resistance formula [5]. Eddy currents in the iron-core and their effects on the inductor model parameters are investigated by a circuit proposed in this paper. The turn-to-turn and turn-to-core capacitances are also considered [6], [7]. Experimental results are presented and compared with the ones calculated by the model to test the validity of the model itself for a laminated iron-core inductor with air gaps.

II. Winding Model

The analytical expressions for the winding ac resistance and leakage inductance of an iron-core inductor as functions of frequency are obtained through the Dowell's approach [5] which takes into account skin and proximity effects in the winding. Thus, the winding ac resistance R_w and leakage inductance L_{ac}^{l} can be expressed as

$$R_w = R_{wdc} A \cdot \left[\frac{e^{2A} - e^{-2A} + 2\sin(2A)}{e^{2A} + e^{-2A} - 2\cos(2A)} + 2\frac{N_l^2 - 1}{3} \cdot \frac{e^{A} - e^{-A} - 2\sin A}{e^{A} + e^{-A} + 2\cos A} \right] \quad (1)$$

and

$$L'_{ac} = R_{wdc}\frac{A}{\omega} \cdot \left[\frac{e^{2A}-e^{-2A}-2\sin(2A)}{e^{2A}+e^{-2A}-2\cos(2A)} + 2\frac{N_l^2-1}{3}\cdot\frac{e^{A}-e^{-A}+2\sin A}{e^{A}+e^{-A}+2\cos A}\right] \quad (2)$$

where R_{wdc} is the winding dc resistance, and A is a dimensionless quantity, which depends on the winding geometry. The first and second terms of (1) represent the skin effect and the proximity effect in the winding, respectively. For a round wire with conductor diameter d, the quantity $A = A_r$ is given by

$$A_r = \left(\frac{\pi}{4}\right)^{\frac{3}{4}} \frac{d^{\frac{3}{2}}}{\delta_w p^{\frac{1}{2}}}, \quad (3)$$

where p is the winding pitch, i.e., the distance between the centers of two adjacent conductors. In (3), δ_w is the skin depth of the wire expressed as

$$\delta_w = \sqrt{\frac{\rho_w}{\pi \mu_o \mu_{rw} f}}. \quad (4)$$

In (4) f is the frequency, ρ_w is the wire electric resistivity, μ_{rw} is the wire relative magnetic permeability (ρ_w = 17.24x10^{-9}Ωm and μ_{rw} = 1 for a copper conductor at 20°C), and μ_0 = 4π 10^{-7} H/m.

The leakage inductance usually represents a small contribution to the total inductance compared to the core inductance [3] and therefore it is neglected in this paper. The winding ac resistance R_w can be modeled by the series Foster circuit depicted in Fig. 2. The parameters of this circuit are fitted to match the Dowell's analytical expression for R_w.

The fitting is performed by an iterative method [4]. The real part of the impedance of the series Foster circuit shown in Fig. 2 is given by

$$R_{sF}(\omega) = R_{wdc} + \sum_{i=1}^{M} \frac{\omega^2 L_i^2 R_i}{R_i^2 + \omega^2 L_i^2} = R_w(\omega) \quad (5)$$

where $\omega = 2\pi f$. Extracting the kth block from (5) yields

$$a_k(\omega) = \frac{\omega^2 L_k^2 R_k}{R_k^2 + \omega^2 L_k^2} \quad (6)$$

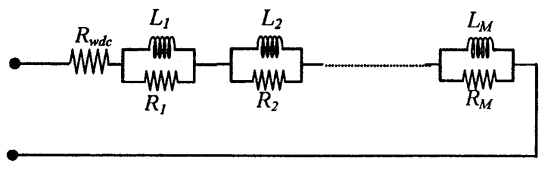

Fig. 2. Series Foster circuit of order M.

where

$$a_k(\omega) = R_w(\omega) - R_{wdc} - \sum_{\substack{i=1 \\ i\neq k}}^{M} \frac{\omega^2 L_i^2 R_i}{R_i^2 + \omega^2 L_i^2} \quad (7)$$

Fixing two frequencies, for each k, it follows that (2)

$$a'_k(\omega'_k) = \frac{\omega'^2_k L_k^2 R_k}{R_k^2 + \omega'^2_k L_k^2} \qquad (k = 1,2,\ldots,M) \quad (8)$$

and

$$a''_k(\omega''_k) = \frac{\omega''^2_k L_k^2 R_k}{R_k^2 + \omega''^2_k L_k^2} \qquad (k = 1,2\ldots,M) \quad (9)$$

From (8) and (9), it follows that

$$R_k = \frac{a'_k a''_k\left(\omega''^2_k - \omega'^2_k\right)}{a'_k \omega''^2_k - a''_k \omega'^2_k} \qquad (k = 1,2\ldots,M) \quad (10)$$

and

$$L_k = R_k \sqrt{\frac{a'_k \omega''^2_k - a''_k \omega'^2_k}{\left(a''_k - a'_k\right)\omega'^2_k \omega''^2_k}} \qquad (k = 1,2\ldots,M) \quad (11)$$

where the terms a'_k and a''_k are calculated by (7).

As the resistance R_{wdc} is known, starting from a set point of the $2M$ series Foster circuit parameters, equations (10) and (11) are used iteratively to update the parameters R_k and L_k until convergence. $2M$ frequencies need to be chosen to determine the $2M$ circuit parameters. The fitting iteration is started at the highest frequency [4].

In this paper, the Foster circuit is fitted by expression (1) calculated for an inductor winding consisting of N_t = 23 turns per layer, N_l = 6 layers with round conductor of diameter d = 1.5 mm. In Fig. 3 the winding ac resistance R_w is plotted as a function of frequency using the Dowell's formula (solid line) and the series Foster circuits of order two and three (dotted and dashed lines, respectively). These circuits have the exact value of resistance at the selected frequencies while they depart from the exact value for the other frequencies. Fig. 4 depicts the relative error in the resistance R_w calculated by the Foster circuits versus frequency (up to 1MHz). As expected, the fitting is better with the circuit of order three, being the relative error much lower in this case. The frequencies assumed for the fitting and the values obtained for the circuit parameters are reported in Table 1.

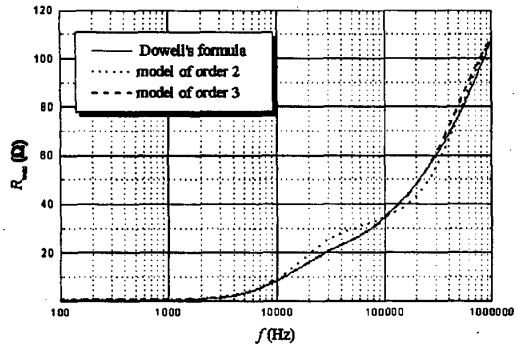

Fig. 3. Winding ac resistance R_w versus frequency.

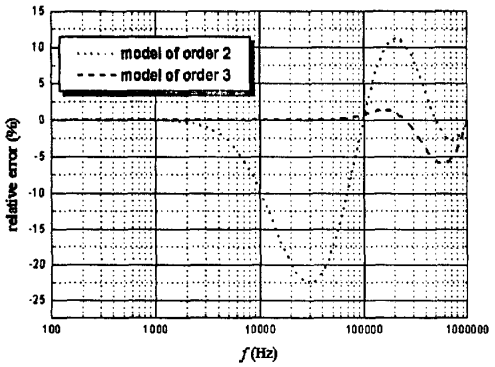

Fig. 4. Relative error in R_w versus frequency.

TABLE I
FOSTER CIRCUIT PARAMETERS

order	2	3
frequencies kHz	0.4, 100, 500, 1000	0.4, 2, 10, 50, 250, 1000
parameters	R_{wdc}=236 mΩ R_1=31.7 Ω L_1=310.91 μH R_2=100.52 Ω L_2=28.8 μH	R_{wdc}=236 mΩ R_1=22.5 Ω L_1=260.24 μH R_2=19.86 Ω L_2=28.5 μH R_3=85.78 Ω L_3=25.26 μH

III. LAMINATED IRON-CORE MODEL

The electromagnetic model for one sheet of the packet which realizes the core is based on a physical approach proposed in [8]. The cross section of a lamination is divided into m regions (as shown in Fig. 5) to simulate eddy currents at the different depths of the sheet. For a more accurate simulation, the region thicknesses should be increased from the surface to the center of the sheet. The magnetic fluxes related to each region and flowing normally to the cross

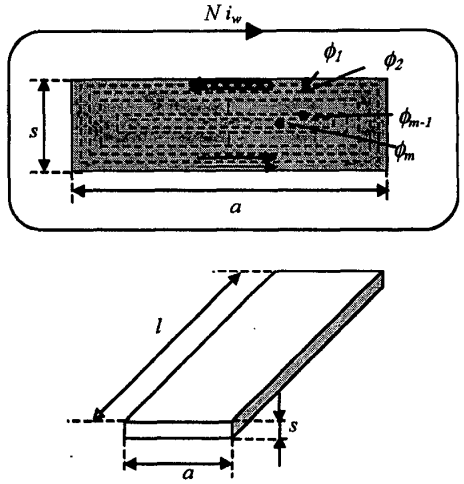

Fig. 5. Lamination and its division into m regions.

section of the sheet are indicated as $\phi_1, \phi_2, \ldots, \phi_m$, respectively. The currents $i_1, i_2, \ldots, i_{m-1}, i_m=0$ represent the currents induced in the considered regions flowing in the cross-sectional plane. In the model, the magnetomotive force Ni_w is due to the external current i_w flowing in the N turns of the coil. If the length of the lamination is much larger than its cross-sectional dimensions, the magnetic flux density and current density fields can be assumed one-dimensional. In particular, the magnetic flux density field exists only inside the lamination with direction perpendicular to the cross section. The interaction between the current and the magnetic flux in a same region is neglected. According to these assumptions and in the case of a nonsaturated laminated iron-core, the magnetic flux ϕ_j in the jth region is a function of the magnetic field intensity H in this region, i.e. it is proportional to the sum of the currents outside the jth region $N i_w + \sum_{\substack{h=1 \\ j\neq 1}}^{j-1} i_h$. The constant of proportionality is the reciprocal of the reluctance $\Re_j = l/(\mu 2 d_j a)$ of the jth region. We have

$$\Re_j \phi_j = N i_w + \sum_{\substack{h=1 \\ j\neq 1}}^{j-1} i_h . \qquad (12)$$

Fig. 6 depicts the regions in which the cross section of the lamination is subdivided, useful for the calculation of the electrical resistance R_h and reluctance $\Re_h$ of each region.

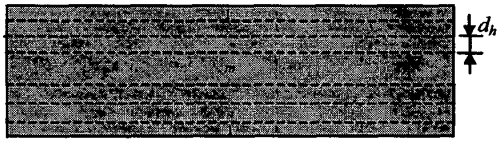

Fig. 6. Simplified regions for calculating electrical resistance and reluctance.

In Fig. 6 the current lines which are parallel to the thickness of the lamination are neglected, being the lamination thickness s much smaller than the a dimension. This hypothesis is the same that is assumed in the analytical solution of the one-dimensional electromagnetic diffusion equation inside the lamination [9].

The current i_h induced in the hth region is obtained from the Faraday's law and Ohm's law as

$$i_h = -\frac{1}{R_h}\sum_{k=h+1}^{m}\frac{d\phi_k}{dt} \tag{13}$$

where $R_h = \rho 2a/(d_h l)$ is the resistance of the hth region.

Equations (12) and (13) can be considered as the equations of the lumped parameter magnetic circuit shown in Fig. 7. In Fig. 7 the magnetomotive force sources are indicated with the symbols used for the independent and dependent voltage sources because of the analogy between magnetomotive force in magnetic circuits and voltage (electromotive force) in electric circuits. This circuit describes the electromagnetic links in the different regions of the lamination and represents a model for time-domain analysis. The solution of the circuit of Fig. 7 gives the fluxes ϕ_j (j = 1,2,..., m). Then the eddy currents i_h (h = 1, 2,..., m-1) can be obtained from (13). This circuit was implemented and solved by a circuit simulator (PSpice) for the laminated iron-core inductor with air gaps depicted in Fig. 8.

The model allows one to calculate the voltage induced across the winding by the magnetic flux as

$$v = Nn\frac{d\phi}{dt} \tag{14}$$

where $N = N_t N_l$ is the turn number of the winding and n is the number of laminations of the packet. In (14) ϕ is the magnetic flux through the cross section of a sheet given by

$$\phi = \sum_{j=1}^{m}\phi_j\,, \tag{15}$$

and the flux through the small space between two adjacent sheets is neglected.

In sinusoidal steady state at radian frequency ω, phasors can be introduced and (14) can be written as

$$\hat{V} = j\omega Nn\hat{\phi}\,. \tag{16}$$

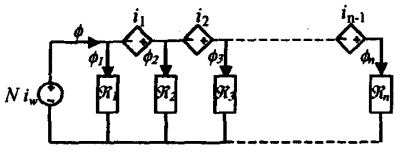

Fig. 7. Model for a lamination.

Let us define the impedance of the inductor as

$$\hat{Z} = \frac{\hat{V}}{\hat{I}_w} = \frac{j\omega Nn\hat{\phi}}{\hat{I}_w}\,. \tag{17}$$

The real and imaginary parts of $\hat{Z}$ represent the core equivalent series resistance R_c (related to the losses due to eddy currents flowing in the core) and the coil main reactance ωL_{ac}^m (related to the magnetic field paths in the core), respectively. The parameters R_c and L_{ac}^m can be calculated at different frequencies by the model shown in Fig. 7.

Analytical expressions for R_c and L_{ac}^m can be obtained through a one-dimensional analysis of the electromagnetic diffusion in a packet of laminations in sinusoidal steady state [1], [9]. In the case of nonsaturated laminated iron-core inductors with air gaps, the expressions for the core equivalent series resistance R_c and main inductance L_{ac}^m are [1]

$$R_c = 2\pi f L_{dc}^m \frac{\delta_c}{s}\frac{\sinh\frac{s}{\delta_c} - \sin\frac{s}{\delta_c}}{\cosh\frac{s}{\delta_c} + \cos\frac{s}{\delta_c}}\,, \tag{18}$$

and

$$L_{ac}^m = L_{dc}^m \frac{\delta_c}{s}\frac{\sinh\frac{s}{\delta_c} + \sin\frac{s}{\delta_c}}{\cosh\frac{s}{\delta_c} + \cos\frac{s}{\delta_c}}\,, \tag{19}$$

where L_{dc}^m is the low-frequency main inductance, s is the thickness of the lamination, and $\delta_c = \sqrt{\rho_c/\pi\mu_e f}$ is the skin depth of the iron sheets, being ρ_c and μ_e the electric resistivity and the equivalent magnetic permeability of the laminated iron-core, respectively. The value of the equivalent magnetic permeability of the EI core, shown in Fig. 8, was calculated as $\mu_e = \mu_c l_c/(l_c + 2\mu_{rc} l_a)$, where l_c is the length of the path consisting of the geometrical axis of the half central limb and that of one of the two outer limbs, 2 l_a is the total air gap and μ_{rc} is the relative permeability of iron.

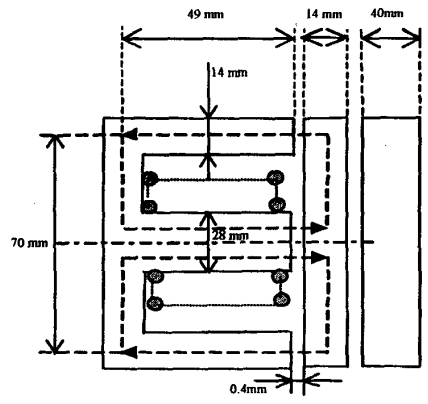

Fig. 8. EI magnetic core and its dimensions.

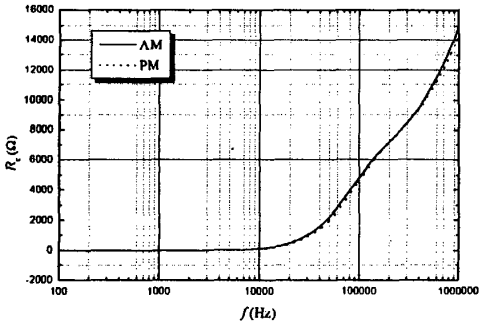

Fig. 9. Equivalent series resistance R_c versus frequency.

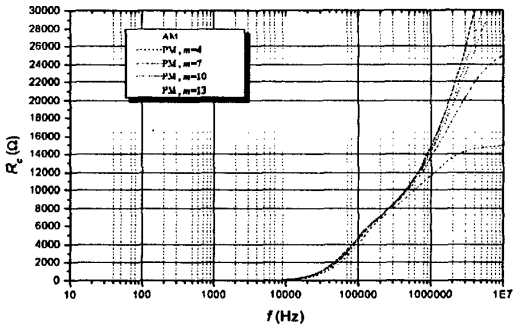

Fig . 11. Equivalent core resistance R_c for different numbers m of regions versus frequency.

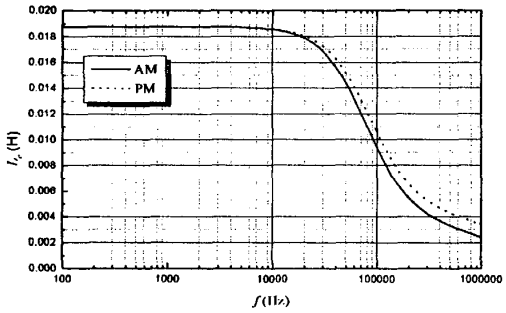

Fig. 10. Main inductance L_{ac}^{m} versus frequency.

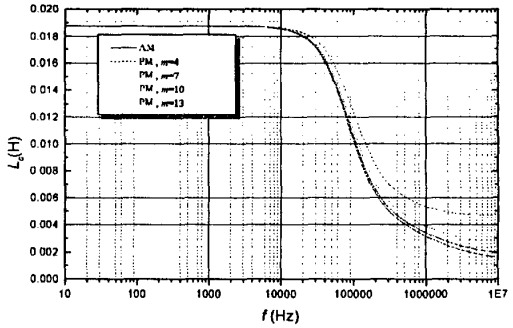

Fig. 12. Main inductance L_{ac}^{m} for different numbers m of regions versus frequency.

TABLE II
MAIN INDUCTOR PARAMETERS

d	1.5 mm
p	1.5 mm
N_l	6
N_t	23
A_{Fe}	1067.36 mm^2
l_c	168 mm
l_a	0.4 mm
μ_e/μ_0	123.53
n	127
L_{dc}^{m}	18.8 mH
R_{wdc}	236 mΩ
f_r	0.103 MHz
C	152.95 pF

TABLE III
CALCULATED ELECTRICAL RESISTANCE AND RELUCTANCE FOR DIFFERENT NUMBER OF REGIONS

m	R mΩ	$\Re$ $H^{-1}m^{-1}10^6$
4	6.2	515.6
7	10.8	902.3
10	15.5	1289.0
13	20.2	1675.8

Figs. 9 and 10 depict the curves R_c and L_{ac}^{m} versus frequency, respectively, calculated for the EI core of Fig. 8 using (18) and (19) (analytical method, AM) and the proposed model (PM) with m = 10 regions of the same thickness. The main parameters of the tested laminated iron-core inductor are reported in Table II.

In the frequency range 100 Hz ÷ 1 MHz, the values obtained by the proposed model are in good agreement with the ones derived by the analytical method when the lamination is divided into 10 regions. In Figs. 11 and 12 the behaviors of the core equivalent resistance and main inductance for different numbers m of regions are shown. It can be noted that the fitting improves with the increasing number of regions. The cases m=10 and m=13 show very similar trends in whole frequency range, so a number of 10 regions for the lamination seems adequate.

In Table III the electrical resistance and reluctance for each examined case of number of regions are reported.

Fig. 13 shows the overall model for the laminated iron-core including the parasitic capacitance C, which is obtained from the inductor self-resonance measurements.

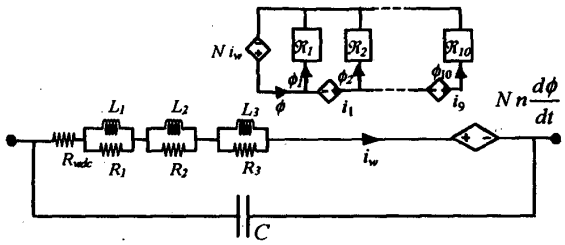

Fig. 13. Overall model for the laminated iron-core inductor.

IV. Experimental Results

The proposed overall model was verified by measurements on a test inductor in the frequency domain. Measurements were carried out on the laminated iron-core inductor with air gaps described in Fig. 8 by an HP 4192A LF Impedance Analyzer (5Hz-13MHz). Fig. 1(b) depicts a series equivalent circuit of the inductor, where the equivalent series parameters R_s and L_s are [3]

$$R_s(\omega)=\frac{R_{ac}}{(1-\omega^2 L_{ac}C)^2+(\omega C R_{ac})^2} \tag{20}$$

and

$$L_s(\omega)=\frac{X_s(\omega)}{\omega}=\frac{L_{ac}(1-\omega^2 L_{ac}C-\frac{CR_{ac}^2}{L_{ac}})}{(1-\omega^2 L_{ac}C)^2+(\omega C R_{ac})^2} \tag{21}$$

where $R_{ac}=R_w+R_c$ and $L_{ac}=L_{ac}^m$. The self-resonant frequency $f_r = \omega_r / (2\pi)$ of an inductor is defined as the frequency at which the reactance X_s is zero. Hence, from (21) the total parasitic capacitance can be calculated as

$$C=\frac{1}{\omega_r^2 L_{ac}(\omega_r)+\frac{R_{ac}^2(\omega_r)}{L_{ac}(\omega_r)}}. \tag{22}$$

The value of total capacitance C is obtained from (22) using the measured self-resonant frequency, and it is assumed to be a constant parameter in the whole range of inductor operating frequencies [1]. Figs. 14 and 15 show the measured (dotted line) and calculated (solid line) results for the test inductor, in terms of R_s and X_s, as a function of frequency.

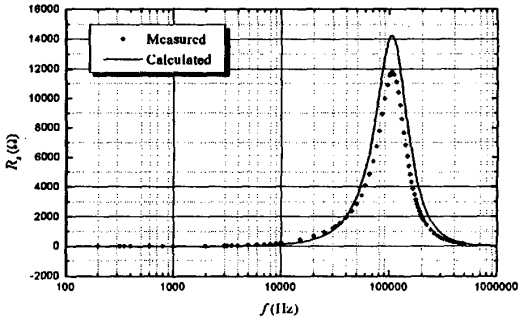

Fig. 14. Measured and calculated R_s versus frequency.

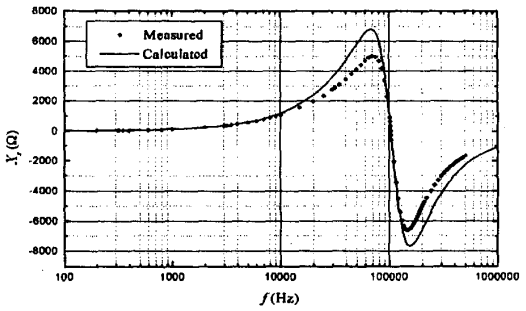

Fig. 15. Measured and calculated X_s versus frequency.

Fig. 16 shows about 100 μs of the dynamic response of the inductor equivalent circuit depicted in Fig. 13, when a voltage rectangular waveform with a frequency of 40 kHz is applied to it. Fig. 16 (a) depicts the behavior of the current absorbed by the inductor, in which the spikes due to the charge and discharge of the capacitive branch are predominant. Fig. 16 (b) shows the current in the inductive branch, which is not triangular as in the case of an ideal inductor.

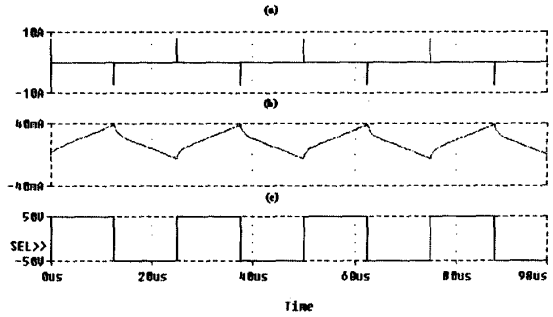

Fig. 16. Simulation results: (a) current absorbed by the inductor, (b) current in the inductive branch, (c) voltage rectangular waveform applied to the inductor.

V. CONCLUSIONS

A model useful to simulate electromagnetic transients of laminated iron-core inductors is presented. The winding is modeled by series Foster circuits of order two and three fitted by the Dowell's resistance formula. Eddy currents in the laminated iron-core and their effects on the inductor model parameters are investigated by the circuit proposed in this paper. The parameter values obtained by the model are compared to those derived from analytical formulae and the agreement between results is good.

The measurements carried out for a laminated iron-core inductor with air gaps are compared to the numerical results obtained by the overall model proposed in this paper. The comparison is made in terms of equivalent series resistance and equivalent series reactance. The agreement is good in a wide frequency range.

The proposed model is suitable for time-domain analysis and simulation results are presented in the case of an inductor supplied by a voltage rectangular waveform.

REFERENCES

[1] U. Reggiani, G. Grandi, G. Sancineto, M.K. Kazimierczuk, and A. Massarini, "High-frequency behavior of laminated iron-core inductors for filtering applications," in *Proc. IEEE-APEC '00*, New Orleans, Louisiana (USA), Feb. 2000, pp. 654-660.

[2] U. Reggiani, G. Grandi, G. Sancineto, G. Serra "Comparison between air-core and laminated iron-core inductors in filtering applications for switching converters," in *Proc. IEEE-CIEP*, Acapulco, Mexico, Oct. 2000, pp. 9-14.

[3] M.K. Kazimierczuk, G. Sancineto, G. Grandi, U. Reggiani, and A. Massarini, "High-frequency small-signal model of ferrite core inductors," *IEEE Trans. Magn.*, vol. 35, no. 5, Sept.. 1999, pp. 4185-4191.

[4] F. De Leon, and A. Semlyen, "Time domain modeling of eddy current effects for transformer transient," *IEEE Trans. Power Delivery*, vol. 8, no.1, Jan. 1993, pp.271-280.

[5] P.J. Dowell, "Effects of eddy currents in transformer windings," *Proc. IEE*, vol. 113, no. 8, Aug. 1966, pp. 1387-1394.

[6] G. Grandi, M.K. Kazimierczuk, A. Massarini, and U. Reggiani, "Stray capacitances of single-layer solenoid air-core inductors," *IEEE Trans. Ind. Applicat.*, vol. 35, no. 5, Sept./Oct. 1999, pp. 1162-1168.

[7] A.Massarini, M.K.Kazimierczuk, and G.Grandi, "Lumped parameter models of single and multiple layer inductors," in *Proc. IEEE-PESC '96*, Baveno (IT), June 1996, pp. 295-301.

[8] Pär Holmberg, "Modelling the transient response of windings, laminated steel cores and electromagnetic power devices by means of lumped circuits," *PhD Thesis*, Uppsala University, 2000.

[9] J. Lammeraner and M. Stafl, *Eddy Currents*. London: Iliffe Books Ltd., 1966.